

Constructing low-dimensional ordinary differential equations from chaotic time series of high/infinite-dimensional systems using radial function-based regression

Natsuki Tsutsumi

Faculty of Commerce and Management, Hitotsubashi University, Japan

Kengo Nakai

The Graduate School of Environment, Life, Natural Science and Technology, Okayama University, Japan

Yoshitaka Saiki

Graduate School of Business Administration, Hitotsubashi University, Japan

(Dated: August 25, 2023)

In our previous study (N. Tsutsumi, K. Nakai and Y. Saiki (2022)) we proposed a method of constructing a system of differential equations of chaotic behavior only from observable deterministic time series, which we will call radial function-based regression (RfR) method. The RfR method employs a regression using Gaussian radial basis functions together with polynomial terms to facilitate the robust modeling of chaotic behavior. In this paper, we apply the RfR method to several types of relatively high-dimensional deterministic time series generated by a partial differential equation, a delay differential equation, a turbulence model, and intermittent dynamics. The case when the observation includes noise is also tested. We have effectively constructed a system of differential equations for each of these examples, which is assessed from the point of view of time series forecast, reconstruction of invariant sets, and invariant densities. We find that in some of the models, an appropriate trajectory is realized on the chaotic saddle and is identified by the Stagger-and-Step method.

I. INTRODUCTION

Scientists have attempted to search for a governing law when they observe an intriguing phenomenon. Kepler's laws of planetary motion are said to be derived by Johannes Kepler, whose analysis of the observations of Tycho Brahe enabled him to establish the laws in the early 17th century. Sir Isaac Newton is said to establish the law of universal gravitation based on experimental observations made previously by Galileo Galilei. The laws are summarized as differential equations. Since then especially for microscopic dynamics of various physical phenomena, the corresponding differential equations have been discovered.

Models of dynamics are constructed primarily via a physical understanding of the phenomena. However, in the last few decades, several approaches have been proposed concerning modeling dynamics from given time series data with the aid of machine learning techniques [1–5]. Although the aim of these approaches is mainly to infer short time series, some models have also succeeded in mimicking dynamical system features such as invariant sets and invariant densities [5].

Some studies [6–9] estimate a system of ordinary differential equations (ODEs) from time series data, which makes it easy to analyze dynamical system features. The above methods require observation time series of all the variables of a system of ODEs to be modeled. For example, they require time series of all three variables x, y, z to construct a data-driven model of the Lorenz 1963 dynamics [10].

There are attempts [11–13] which derive a system of ODEs from scalar time series. The observable variable and its time derivatives are used for the model variables. In [14], the problem with observational (Gaussian or white) noise is investigated. In the series of studies, prior knowledge of the background dynamics is used to choose basis functions for the

gression, and the method is not appropriate for modeling for practical purposes.

Recently we proposed a simple method of constructing a system of ODEs of chaotic behavior based on the regression only from observable scalar time series data with the basis functions unchanged [15]. Independent of the dynamics, we employ spatially localized radial basis functions in addition to polynomial basis functions for the regression. We can say that our method is the only method that can model a system of ODEs from scalar time series data which is applicable to various dynamics without assuming the knowledge of the background dynamics. Furthermore, we should note that the capability of the forecasting is not limited to a short time series but a density distribution created using a long time series.

Unlike prior studies [6–8] our radial function-based regression (RfR) method proposed in [15] is applicable even when the time derivative of each variable is not approximated by the low-order polynomials of variables. We exemplified that our RfR method worked well for a time series of one variable (x) of the typical and simple chaotic dynamics given by the Lorenz system, and evaluated the constructed data-driven model in detail. Our model construction using the RfR method has several advantages in that the method simultaneously meets the following: a model variable is physically understandable; a model can be constructed even when the number of observable variables is limited and even when no knowledge of the governing system is given. The RfR method allows us to construct a model using physically understandable variables.

In this research, we present the applicability of our RfR method to complex dynamics described by infinite or finite but high-dimensional systems including the Kuramoto-Sivashinsky equation [16], the Mackey-Glass equation [17], the shell model of fluid turbulence [18] and intermittent dynamics described by the coupled Rössler equation [19].

The Kuramoto-Sivashinsky equation is the partial differential equation system that can reveal spatio-temporal chaos; the Mackey-Glass equation is the delay differential equation which is a model of feedback control of blood cells; the shell model turbulence is a system of high-dimensional ODEs of complex variables which mimic the spectral equation in Fourier space of the Navier-Stokes system; the coupled Rössler equation is an ordinary differential equation system that can show intermittent behavior. Note that for the shell model turbulence, we use time series data of a variable that does not appear in the original system. It is common that observable data includes noise. So in the case of the Kuramoto-Sivashinsky equation, the effect of noise added to the observation data is also investigated.

We assume there exists an unknown system of N dimensional ODEs called an original system concerning an unknown variable \mathbf{x} :

$$\frac{d\mathbf{x}}{dt} = \mathbf{f}(\mathbf{x}), \quad (1)$$

or an infinite dimensional system such as a partial differential equation and delay differential equation whose dynamics can be approximated well by Eq. 1. In this paper the above-mentioned examples are chosen as Eq. 1. We can observe some of the components of the variable \mathbf{x} , or more generally

$$w_i = g_i(\mathbf{x}), \quad i = 1, \dots, I. \quad (2)$$

Note that w_i does not necessarily be described as a function of \mathbf{x} , but can be an integrated value of \mathbf{x} . The case when w_i includes noise is also investigated. We are unable to reconstruct the original system Eq. 1 itself from given time series data unless all the components of the variable \mathbf{x} in Eq. 1 and their time series are known. We assume that there exists a system of D dimensional ODEs:

$$\frac{d\mathbf{X}}{dt} = \mathbf{F}(\mathbf{X}), \quad (3)$$

where the first I components of the variable \mathbf{X} are $X_i = w_i$ ($i = 1, \dots, I$) and the rest of X_i ($i = I+1, \dots, D$) are created from the delay-coordinates of some w_i [20, 21]. The aim of our proposed method is to model Eq. 3 that can describe the behavior of the observable variables w_i ($i = 1, \dots, I$) as components of the variable \mathbf{X} which is made only by the observable variable w_i .

By the RfR method, we have succeeded in the modeling of dynamics even when the right-hand side of Eq. 3 cannot be described by low-order polynomials. This is primarily because of the introduction of the Gaussian radial basis functions. It allows us to ease the modeling of a chaotic attractor for a variety of dynamics. However, even if the obtained data-driven model does not have a chaotic attractor, we can generate a trajectory staying in the chaotic saddle by employing the Stagger-and-Step method [22]. The Stagger-and-Step method is applied to create a long chaotic trajectory of the data-driven model for the shell model turbulence and the Kuramoto-Sivashinsky equation with observation noise. See Appendix A for the detail.

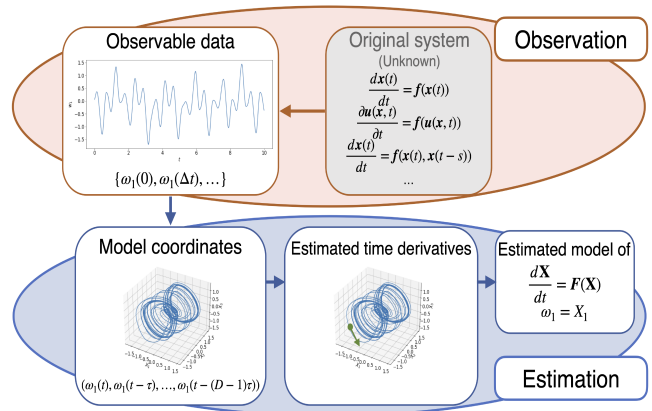


FIG. 1. Outline of the proposed radial function-based regression (RfR) method for constructing a system of ODEs.

The rest of the paper is organized as follows. In Section II, we introduce the proposed method for deriving a system of ODEs. In Section III, we demonstrate the settings of the construction of a data-driven model for each of the examples. In Section IV, we assess the constructed data-driven models. Concluding remarks are given in Section V.

II. METHOD: RADIAL FUNCTION-BASED REGRESSION (RfR)

As shown in Fig. 1, our aim is to construct a system of D dimensional ODEs Eq. 3 based only on some observable deterministic time series w_i ($i = 1, \dots, I$) of length T with time step Δt , and data size $N_T = T/\Delta t$. The steps of the proposed method (RfR) are outlined below:

- i. Choose the delay-coordinate variable: delay-time τ and dimension D
- ii. Estimate the time derivative at each sample point using the Taylor approximation
- iii. Choose the basis function¹ used in Step iv
- iv. Perform linear regression at sample points with ridge regularization
- v. Assess the model quality according to the reproducibility of the delay structure in a generated model trajectory

A. Choice of model variables

For practical reasons, the number of observable variables is small, when compared to the dimension of the background dynamical system. To describe dynamics, we generate a higher

¹ We do not assume some particular vector space in advance as is usual in the literature for machine learning.

dimensional variable by introducing the delay-coordinates of limited observables such as $(w_1(t), w_1(t - \tau), w_1(t - 2\tau), \dots, w_1(t - (D - 1)\tau))$.

B. Estimating the time derivative

We apply the Taylor approximation to estimate the time derivative at each sample point $\mathbf{X}(\tilde{t})$ based only on discrete time points of a trajectory $\mathbf{X}(t)$ ($t = \dots, \tilde{t} - \Delta t, \tilde{t}, \tilde{t} + \Delta t, \dots$). In our computations, we employ the sixth order approximation:

$$\begin{aligned} \frac{d\mathbf{X}(\tilde{t})}{dt} &\approx \frac{1}{60l\Delta t} \{ \mathbf{X}(\tilde{t} + 3l\Delta t) - 9\mathbf{X}(\tilde{t} + 2l\Delta t) \\ &+ 45\mathbf{X}(\tilde{t} + l\Delta t) - 45\mathbf{X}(\tilde{t} - l\Delta t) + 9\mathbf{X}(\tilde{t} - 2l\Delta t) \\ &- \mathbf{X}(\tilde{t} - 3l\Delta t) \}, \end{aligned}$$

where $l (\geq 1)$ is a positive integer to determine the points to estimate the time derivative at $\mathbf{X}(\tilde{t})$, that is, points at every $l\Delta t$ time step are used.

When the observable data includes noise, we choose a large value of l to estimate the time derivative, which allows us to avoid high-frequency oscillations. In that case, we need to employ the high (*e.g.*, sixth) order Taylor approximation. Note that if the observable data does not include noise, we do not need to use such a high order formula. See Appendix C for the estimation of the time derivative at each sample point when noise is added to the time series.

C. Choice of basis function

We construct a model Eq. 3 through the linear regression of the following form:

$$F_k(\mathbf{X}) \approx \tilde{\beta}_0^k + \sum_{d=1, \dots, D} \tilde{\beta}_d^k X_d + \sum_{j=1, \dots, J} \tilde{\beta}_{D+j}^k \phi_j(\mathbf{X}), \quad (4)$$

where $F_k(\mathbf{X})$ is the k th component of $\mathbf{F}(\mathbf{X})$ in Eq. 3, $\tilde{\beta}^k = (\tilde{\beta}_0^k, \tilde{\beta}_1^k, \dots, \tilde{\beta}_{D+J}^k)$ is a set of estimated parameters and

$$\phi_j(\mathbf{X}) = \exp\left(\frac{-\|\mathbf{X} - c_j\|^2}{\sigma^2}\right),$$

is the Gaussian radial basis function, where $\|\cdot\|$ denotes the l^2 norm, $c_j \in \mathbb{R}^D$ is the coordinate of the j th center point ($j = 1, \dots, J$), and σ^2 is the parameter that determines the deviation of ϕ_j .

In this RfR method, c_j is distributed as lattice points with grid size δ_{grid} . For a given integer m explained below, we consider c_j such that there exists a data point in the $(m - 1)\delta_{grid}$ -neighborhood. An increase in δ_{grid} results in a decrease in the number of center points and a decrease in the required computational resources.

For a given δ_{grid} , σ^2 is determined as

$$\sigma^2 := \frac{((m - 1)\delta_{grid})^2}{-\log_e p},$$

where m is the degree of the corresponding B-spline basis function and $p (> 0)$ is a small value. When we set $m = 3$, and $p = 0.1$, then $(m - 1)^2 / (-\log_e p) \approx 1.7372$. See Kawano and Konishi [23] for more details.

D. Ridge regression

For determining the coefficients in Eq. 4 we obtain the minimizer of the following function

$$L(\mathbf{b}) = \frac{1}{2n} \|\mathbf{y} - A\mathbf{b}\|^2 + \frac{\lambda}{2} \|\mathbf{b}\|^2,$$

where n is the size of regression data, \mathbf{y} represents the standardized time derivative (see the left-hand side of Eq. 3), λ is a parameter determining the strength of regularization, and A is $n \times (D + J)$ matrix whose i -th row is $(X_1(t_i), \dots, X_D(t_i), \phi_1(\mathbf{X}(t_i)), \dots, \phi_J(\mathbf{X}(t_i)))$ (see Eq. 4). The regularization is used to prevent overfitting primarily due to the introduction of the Gaussian radial basis functions.

The ridge estimator attaining the minimum of $L(\mathbf{b})$ is written as follows:

$$(A^T A + n\lambda I)^{-1} A^T \mathbf{y},$$

where I is the identity matrix and A^T is the transpose of A . Due to the limited computational resources, it is hard to use all data of size N_T . We randomly choose samples of size n among N_T for regression.

E. Evaluation of the model

For assessing the model quality we confirm the delay structure in the model trajectory. When the number of observable variable is one, the model trajectory should satisfy the following:

$$X_1(t) \approx X_2(t + \tau) \approx \dots \approx X_D(t + (D - 1)\tau). \quad (5)$$

The hyper-parameters such as a regularization parameter and grid size are selected adequately based on the level of the reconstruction of the delay structure.

F. Choice of parameters

Table I depicts parameter settings that will be employed in the modeling in Sections III and IV. The parameter δ_{grid} should correspond to a scale of the variable ω_i in Eq. 2. Hence, ω_i is standardized in our modeling to avoid the adjustment. For the choice of parameters we consider the followings:

	KS	MG	SM	CR	n-KS
D	5	7	6	6	5
τ	0.12	0.5	18	0.4	0.12
m	3				
p	0.1				
δ_{grid}	0.50	0.25	0.25	0.25	0.50
J	19,322	241,402	693,749	91,393	35,179
l	1	1	1	1	9
λ	10^{-7}	10^{-7}	10^{-12}	10^{-7}	10^{-4}
n	50,000				
I	1	1	1	2	1
N_T	10^6				
Δt	0.01	0.01	1.0	0.1	0.01

TABLE I. **Sets of parameters.** They are used for the modelings of the Kuramoto-Sivashinsky equation (KS), Mackey-Glass equation (MG), the shell model of fluid turbulence (SM), the coupled Rössler equation (CR), and the Kuramoto-Sivashinsky equation with noise (n-KS).

- The dimension D of the model is selected to be bigger than the expected attractor dimension. But small dimension D is effective for the computations.
- The delay time τ is selected based on the decay of correlation of a variable $X_1(t)$. τ is chosen to meet that the correlation between $X_1(t)$ and $X_1(t - \tau)$ is around 0.5 (See Appendix B).
- The parameter l used for estimating the time derivative at each sample point is chosen larger when the observable data includes noise with larger amplitude (See section II B).
- The number of center points J is determined by the settings of δ_{grid} and m (See section II C).
- The number of regression points n is not very sensitive and fixed as 50,000 (See section II D).
- The regularization parameter λ is chosen so that the reproducibility of the delay structure is successful (See section II E), but is not very sensitive.

III. EXAMPLE DYNAMICS TO BE MODELED

A. PDE dynamics: Kuramoto-Sivashinsky equation

We model differential equations using a scalar time series of the Kuramoto-Sivashinsky equation [16] under periodic boundary conditions:

$$\frac{\partial u}{\partial t} = -\frac{\partial^2 u}{\partial x^2} - \nu \frac{\partial^4 u}{\partial x^4} + \left(\frac{\partial u}{\partial x}\right)^2, \mathbb{T} \times \mathbb{R}^+$$

where $\mathbb{T} = [0, 2\pi)$, and ν corresponds to the viscosity parameter and is set as $\nu = 0.02150$. For creating a training time series, we use the Fourier spectral method with 32 modes, and

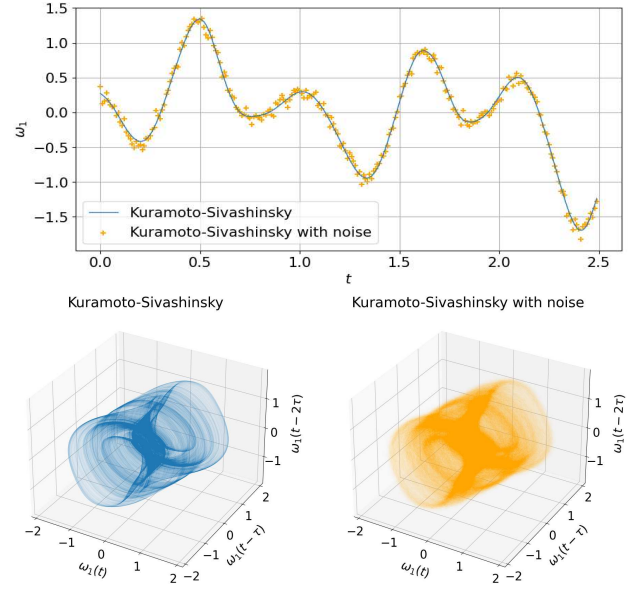


FIG. 2. **Time series of ω_1 of the Kuramoto-Sivashinsky equation and that with observation noise.** The lower panels show corresponding longer trajectories in $(\omega_1(t), \omega_1(t - \tau), \omega_1(t - 2\tau))$ coordinate. The blue line represents the time series of ω_1 of the Kuramoto-Sivashinsky equation and the orange points represent noised observable data.

obtain the following form of ODEs by assuming some symmetry [16]:

$$\frac{da_k}{dt} = (k^2 - \nu k^4)a_k + \frac{k}{2} \left(\sum_{m=k-32}^{-1} a_{-m}a_{k-m} + \sum_{m=1}^{k-1} a_m a_{k-m} + \sum_{m=k+1}^{32} a_m a_{m-k} \right), k = 1, \dots, 32.$$

We assume the number of observable variables in Eq. 2 is $I = 1$, and the variable is $\omega_1 = a_1(t)$, where $a_1(t)$ is a variable of the original Kuramoto-Sivashinsky equation. We set the model coordinate \mathbf{X} in Eq. 3 as $\mathbf{X}(t) = (\omega_1(t), \omega_1(t - \tau), \dots, \omega_1(t - 4\tau))$, where $\tau = 0.12$. See Fig. 2 for a short time series and a long trajectory in $(\omega_1(t), \omega_1(t - \tau), \omega_1(t - 2\tau))$.

B. Time-delay dynamics: Mackey-Glass equation

We deal with a delay differential equation called the Mackey-Glass equation [17]:

$$\frac{dx(t)}{dt} = 2 \frac{x(t-2)}{1+x(t-2)^{9.65}} - x(t).$$

This is also an infinite-dimensional system, but it has a finite-dimensional attractor. We assume the number of observable variables in Eq. 2 is $I = 1$, and the variable is $\omega_1 = x(t)$,

where $x(t)$ is a variable of the original Mackey-Glass equation. We set the model coordinate as \mathbf{X} in Eq. 3 as $\mathbf{X}(t) = (\omega_1(t), \omega_1(t - \tau), \dots, \omega_1(t - 6\tau))$, where $\tau = 0.5$.

C. Turbulence dynamics: shell model of fluid turbulence

We model a system of differential equations using the time series of the shell model of fluid turbulence [18, 24]. The system is a complex-valued differential equation, but we examine a real-valued scalar time series of an absolute value of one complex variable of the following system of differential equations:

$$\begin{aligned} & \left(\frac{du_j}{dt} + \nu k_j^2 \right) u_j \\ &= i(c_j^{(1)} u_{j+2}^* u_{j+1}^* + c_j^{(2)} u_{j+1}^* u_{j-1}^* + c_j^{(3)} u_{j-1}^* u_{j+1}^*) \\ &+ f \delta_{j,1}, \quad (1 \leq j \leq 9) \end{aligned}$$

where $*$ denotes the complex conjugate, f is a time-independent force, ν is the kinematic viscosity, $\delta_{j,l}$ is Kronecker's delta ($l \in \mathbb{N}$), and t is time. The real constants $c_j^{(1)}, c_j^{(2)}, c_j^{(3)}$ ($1 \leq j \leq 9$) are given as $c_j^{(1)} = k_j, c_j^{(2)} = -\delta k_{j-1}, c_j^{(3)} = (\delta - 1)k_{j-2}$ except for $c_1^{(2)} = c_1^{(3)} = c_2^{(3)} = c_{9-1}^{(1)} = c_9^{(1)} = c_9^{(2)} = 0$.

By using a scalar time series of $w_1(t) = |u_3(t)|$ for $f = 0.005(1 + i)$ and $\nu = 0.00251$, we construct a data-driven model by employing the six dimensional variable $\mathbf{X}(t) = (w_1(t), w_1(t - \tau), \dots, w_1(t - 5\tau))$, where $\tau = 18$.

D. Intermittency dynamics: the coupled Rössler equation

We model a system of differential equations using intermittent time series of the coupled Rössler equation [25]:

$$\begin{cases} \frac{dx_1}{dt} = -y_1 - z_1 + \varepsilon(x_2 - x_1) \\ \frac{dy_1}{dt} = x_1 + ay_1 \\ \frac{dz_1}{dt} = f + x_1 z_1 - cz_1 \\ \frac{dx_2}{dt} = -y_2 - z_2 + \varepsilon(x_1 - x_2) \\ \frac{dy_2}{dt} = x_2 + ay_2 \\ \frac{dz_2}{dt} = f + x_2 z_2 - cz_2, \end{cases} \quad (6)$$

where $(a, c, f, \varepsilon) = (0.15, 10, 0.2, 0.06)$. This system is known for the so-called on-off intermittency, nonregular switchings between laminar and bursting states. Each of the states is characterized by the difference between two oscillators (x_1, y_1, z_1) and (x_2, y_2, z_2) . To characterize the switching, we focus on the difference between x_1 and x_2 . Due to the nonuniformity of the value in the differ-

ence, modeling using the difference variable is difficult. Hence, we use two training variables x_1 and x_2 as ω_1 and ω_2 , and see the difference. Then we use their delayed variables $(X_1(t), X_2(t), X_3(t), X_4(t), X_5(t), X_6(t)) = (x_1(t), x_2(t), x_1(t - \tau), x_2(t - \tau), x_1(t - 2\tau), x_2(t - 2\tau))$, where $\tau = 0.4$.

E. PDE dynamics with noise

We model using time series data of the Kuramoto-Sivashinsky equation with the Gaussian noise whose standard deviation is $0.5948 \cdot 0.10$, where 0.5948 is the standard deviation of the ω_1 variable of the Kuramoto-Sivashinsky equation. See Fig. 2 for a short time series and a long trajectory in $(\omega_1(t), \omega_1(t - \tau), \omega_1(t - 2\tau))$. By adding observation noise to the Kuramoto-Sivashinsky dynamics, the local structures are blurred.

IV. RESULTS

In this section, we assess the constructed data-driven models. In section IV A, we assert that we have succeeded in predicting short-time series and that the data-driven models can reconstruct long trajectories and density distribution. We also evaluate the validity of the model by confirming the delay structure of the data-driven models. In section IV B, we assess the stability of each model chaotic invariant set: chaotic attractor or chaotic saddle. We concentrate on the case when the constructed data-driven model does not have a chaotic attractor in section IV C. In section IV D, we assert that the data-driven model for the coupled Rössler equation can reconstruct intermittency.

A. Basic properties of the models

In this section, we evaluate the basic properties of each data-driven model in comparison to those of the corresponding actual dynamics. We find that a time series inference of X_1 can successfully be applied for a short time. Figure 3-a,d,g,j and m depict examples of predicted trajectories, each of which approximates the actual one for a certain amount of time. The growth of error in each model is unavoidable because of the chaotic property of the actual dynamics. We also confirm by calculating a long trajectory that the chaotic invariant set of each data-driven model resembles that of the actual one. Figure 3-b,e,h,k and n depict projections of long trajectories. For three data-driven models for the Kuramoto-Sivashinsky equation, the Mackey-Glass equation, and the coupled Rössler equation the obtained chaotic invariant sets are attractors, and model trajectories are created by forward-time integration of the models. For the case of the shell model and the Kuramoto-Sivashinsky equation with noise, we describe how to create an appropriate model trajectory in section IV C. Furthermore, we demonstrate that data-driven models can reconstruct statistical quantities. In Fig. 3-c,f,i,l and o

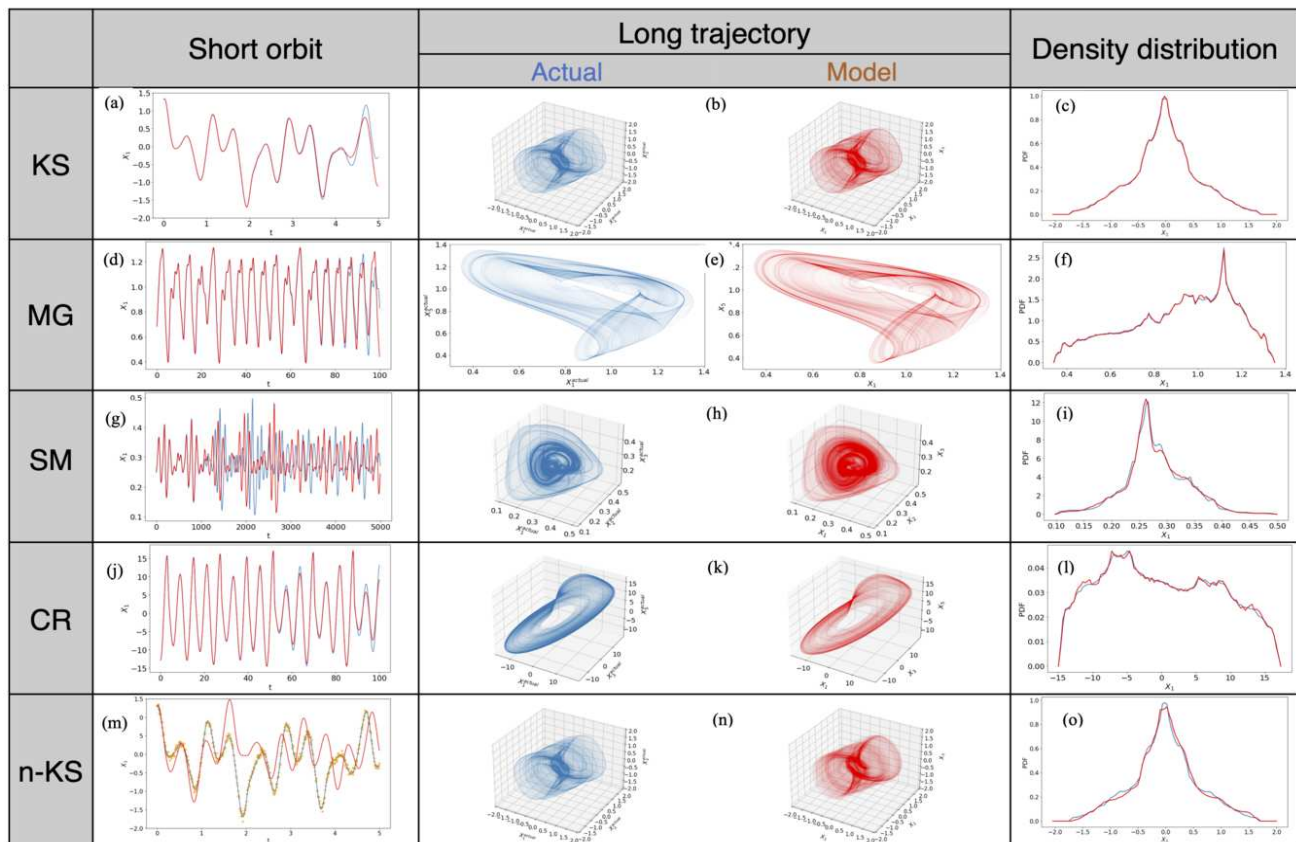


FIG. 3. **Basic properties of a data-driven model for each case (Kuramoto-Sivashinsky equation (KS), Mackey-Glass equation (MG), the shell model of fluid turbulence (SM), the coupled Rössler equation (CR), and Kuramoto-Sivashinsky equation with noise (n-KS)).** The left panels show short trajectories of X_1 , the center panels show long trajectories, and the right panels show density distributions of X_1 . In each panel blue and red indicate the cases for the actual and the model, respectively. See Appendix D for the prediction of short time orbits from various initial conditions.

we show a density distribution computed from a model trajectory $\{X_1(t)\}$ which coincides with that computed from the actual dynamics. We can also see the validity of each model by confirming that short time inference from various initial conditions is successful. See Appendix D that shows the comparison of model time series with actual ones for each of the four models.

Recall that in our modeling we employ a delay-coordinate variable $X(t)$. Hence, the relation (5) should hold for a model to be suitable. By measuring the degree of the delay structure reconstruction, we can assess the constructed model. Relations shown in Fig. 4-a,c,e,g and i represent successful reconstructions of delay structure among time series $X_1(t)$, $X_2(t + \tau)$, \dots , $X_D(t + (D - 1)\tau)$ (for the coupled Rössler equation, $X_1(t)$, $X_3(t + \tau)$ and $X_5(t + 2\tau)$). Figure 4-b,d,f,h and j show density distributions of $X_1(t) - X_2(t + \tau)$ in each data-driven model (for the coupled Rössler equation, $X_1(t) - X_3(t + \tau)$). The degree of the reconstruction for the Kuramoto-Sivashinsky equation with noise is lower than that of the others, due to observation noise.

B. Stability of a chaotic invariant set

Our data-driven model is constructed using trajectory points on a chaotic attractor. Therefore, the model cannot describe dynamics far from the attractor. However, we find that the model can substantially describe dynamics outside the model attractor on which the trajectory points are reconstructed.

We focus on an invariant set outside the model attractor whose corresponding set does not exist in the original system. For many successful cases, we observe that outside the model attractor, there exists a ghost hyperbolic invariant set such as a fixed point or a periodic orbit that is $D - 1$ dimensionally stable, and its stable manifold forms a basin boundary of the model attractor, that is, a point in the basin will be attracted to the model attractor. In some cases, a model attractor has a global basin, and in other cases, there exist no model attractors.

For each case of the Kuramoto-Sivashinsky equation, the Mackey-Glass equation and the coupled Rössler equation a model has a chaotic attractor, and the attractor of a model for the coupled Rössler equation is a global attractor. For the shell model of fluid turbulence and the Kuramoto-Sivashinsky

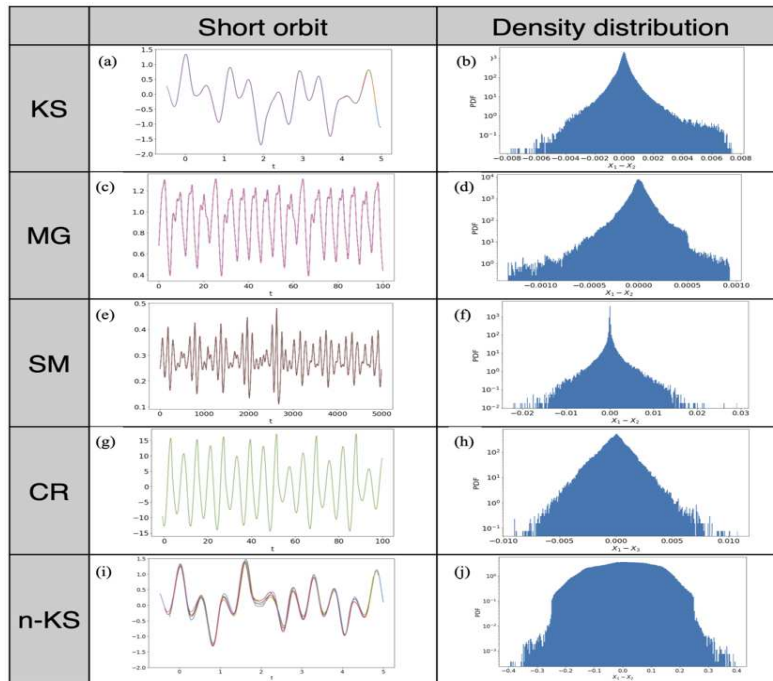


FIG. 4. Delay structures in each data-driven model (Kuramoto-Sivashinsky equation (KS), Mackey-Glass equation (MG), the shell model of fluid turbulence (SM), the coupled Rössler equation (CR), and Kuramoto-Sivashinsky equation with noise (n-KS)). The left panels show short trajectories of $X_1(t)$, $X_2(t + \tau)$, $X_3(t + 2\tau)$, \dots , $X_D(t + (D - 1)\tau)$ ($X_1(t)$, $X_3(t + \tau)$, $X_5(t + 2\tau)$ for CR) for the same time interval as that in Fig. 3 (left). The right panels show density distributions of $X_1(t) - X_2(t + \tau)$ ($X_1(t) - X_3(t + \tau)$ for CR) in logarithmic scale in the vertical axis, and the distributions are localized around zero in comparison with the amplitudes of the fluctuations. The results show the reproducibility of delay structures expected to satisfy for the models to be valid. Hence, the discrepancies in the time series in Fig. 3 (left) are considered to be due to the sensitive dependence on initial conditions of chaotic dynamics.

equation with noise, a model attractor does not exist. Even though we can create a long trajectory that stays in the model chaotic saddle by using the Stagger-and-Step method which is described in the following section IV C.

C. Stagger-and-Step method

As is commonly the case in the model of chaotic dynamics, a long-term trajectory simply created from the model does not absolutely replicate the original dynamics, even though the short time trajectories from multiple initial conditions behave adequately. In this section, we describe a situation and explain how to generate an appropriate long trajectory by employing the data-driven model of the shell model as an example.

Recall that the turbulence shell model has a chaotic attractor, and the data-driven model is constructed from a scalar time series of a trajectory on the chaotic attractor. However, the original chaotic attractor is not reconstructed as a model chaotic attractor but reconstructed as a model chaotic saddle.

A trajectory on a chaotic saddle from almost every initial condition does not stay in the neighborhood of the chaotic saddle. However, there exists an arbitrary long trajectory staying in the neighborhood, which we approximately create as segments of appropriate short trajectories satisfying the constraint of the delay structure explained in section II E. The nu-

merical method we employ to generate such a long trajectory is the Stagger-and-Step method [22]. We create a trajectory at least time length $T = 1,000,000$ on a model chaotic saddle and confirm that the trajectory reconstructs a statistical property as well as the actual short orbit (Figs. 3 and 4).

In the case of the Kuramoto-Sivashinsky equation with noise, we have also succeeded in generating a model trajectory on a chaotic saddle by employing the method. See Appendix A for the details of the Stagger-and-Step method.

D. Intermittency

One of the features of the coupled Rössler equation (6) is that the two different oscillators can depict an intermittent behavior between laminar and bursting states through mutual interactions. We can observe the intermittency by seeing the fluctuation of $x_1 - x_2$.

Figure 5 depicts short-time trajectories of $X_1(t) - X_2(t)$ with those of the actual trajectories. We obtain the distribution of the lasting time of the laminar state $|x_1 - x_2| < C$ for some $C > 0$ sufficiently small. The distribution obtained by the model is depicted in Fig. 6 when $C = 1$. The tail of the distribution obeys a power law, which is comparable to that from the actual coupled Rössler equation. Note that it is hard to model the intermittent dynamics because of the nonuniform

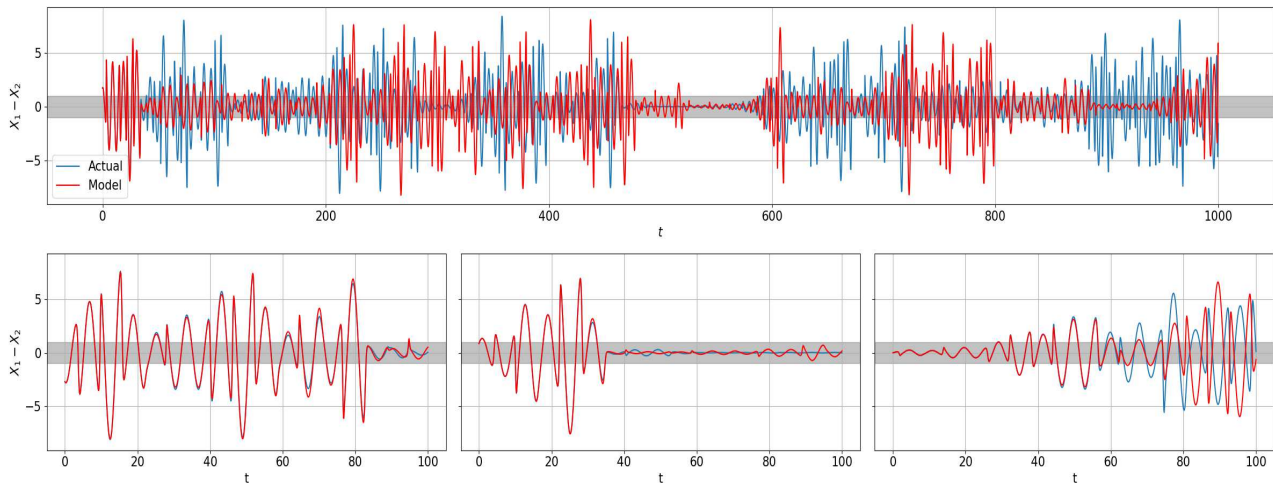


FIG. 5. **Four time series of $X_1 - X_2$ (model) from different initial conditions of a single data-driven model are shown together with that of the actual dynamics (actual) of the coupled Rössler equation.** Each panel illustrates a time series showing intermittency between a laminar state with weak fluctuations $|X_1 - X_2| < C$ ($C = 1$) (colored in gray) and a bursting state with large fluctuations. Each panel shows a different trajectory of a data-driven model together with the corresponding actual trajectory. Switchings between laminar and bursting states can be predicted by the model.

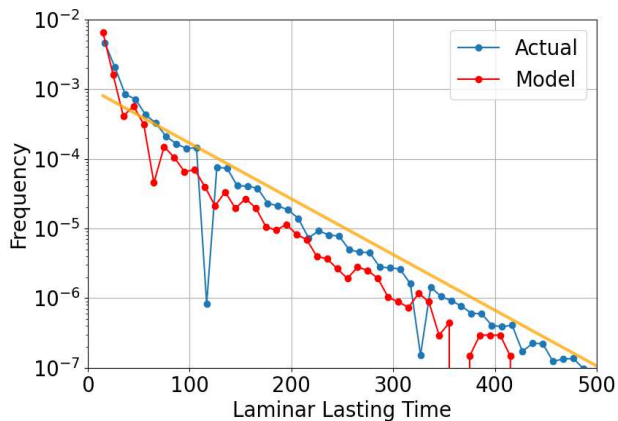


FIG. 6. **The distribution of laminar lasting time for the model is shown together with that of the actual system in a semi-log scale for the coupled Rössler system.** The Laminar lasting time distribution of $X_1 - X_2$ computed from the model trajectory is displayed together with that from the actual system. The orange line has a slope of -0.008 . The distribution of a model is obtained from multiple numerical computations of total time length $T = 750,000,000$ for the actual data, and $T = 4,330,000$ for the model.

mity when the observable variable is limited to the difference between two variables $x_1 - x_2$.

V. CONCLUDING REMARKS

We have succeeded in constructing various differential equations only from observable time series of the limited

number of variables by the RfR method proposed in our previous paper [15]. Our attempts in this study include the dynamics of a partial differential equation, a delay differential equation, a shell model of fluid turbulence, and intermittent dynamics of coupled differential equations. The case when noise is added to the observation is also tested. Each data-driven model is shown to have a trajectory and density distribution, both of which approximate the actual ones. The existence of the model attractor is investigated, and we create a model trajectory by applying a Stagger-and-Step method when an appropriate trajectory is realized not on the model attractor but on the model chaotic saddle.

In order to overcome the limitation of the number of observable variables, we employ the delay-coordinate of the observable variable(s) as a model variable, and it is also useful to test the validity of a model trajectory.

Remarkably, we can model a system of ODEs by employing the RfR method, even if we do not have knowledge of the system in advance. As a practical application, we can apply our method to construct a system of ODEs from time series of macroscopic variables of complex phenomena, e.g. modeling turbulent mean flow or climate dynamics using observable macroscopic variables.

ACKNOWLEDGEMENT

YS was supported by the JSPS KAKENHI Grant No.19KK0067, 21K18584 and 23H04465, and JSPS Bilateral Open Partnership Joint Research Projects JPJSBP120229913. KN was supported by the JSPS KAKENHI Grant No.22K17965 and JST PRESTO 22724051. The computation was carried out using the JHPCN (jh220007 and jh230028)

-
- [1] R. T. Chen, Y. Rubanova, J. Bettencourt, and D. K. Duvenaud, Neural ordinary differential equations, *Advances in Neural Information Processing Systems* **31**, 6571 (2018).
- [2] J. Pathak, Z. Lu, B. R. Hunt, M. Girvan, and E. Ott, Using machine learning to replicate chaotic attractors and calculate lyapunov exponents from data, *Chaos* **27**, 121102 (2017).
- [3] K. Nakai and Y. Saiki, Machine-learning inference of fluid variables from data using reservoir computing, *Phys. Rev. E* **98**, 023111 (2018).
- [4] K. Nakai and Y. Saiki, Machine-learning construction of a model for a macroscopic fluid variable using the delay-coordinate of a scalar observable, *Discrete Contin. Dyn. Syst. S* **14**, 1079 (2021).
- [5] M. U. Kobayashi, K. Nakai, Y. Saiki, and N. Tsutsumi, Dynamical system analysis of a data-driven model constructed by reservoir computing, *Phys. Rev. E* **104**, 044215 (2021).
- [6] E. Baake, M. Baake, H. G. Bock, and K. M. Briggs, Fitting ordinary differential equations to chaotic data, *Phys. Rev. A* **45**, 5524 (1992).
- [7] W.-X. Wang, R. Yang, Y.-C. Lai, V. Kovanis, and C. Grebogi, Predicting catastrophes in nonlinear dynamical systems by compressive sensing, *Phys. Rev. Lett.* **106**, 154101 (2011).
- [8] S. L. Brunton, J. L. Proctor, and J. N. Kutz, Discovering governing equations from data by sparse identification of nonlinear dynamical systems, *Proc. Natl. Acad. Sci.* **113**, 3932 (2016).
- [9] K. Champion, B. Lusch, J. N. Kutz, and S. L. Brunton, Data-driven discovery of coordinates and governing equations, *Proc. Natl. Acad. Sci.* **116**, 22445 (2019).
- [10] E. N. Lorenz, Deterministic nonperiodic flow, *J. Atmos. Sci.* **20**, 130 (1963).
- [11] G. Gouesbet, Reconstruction of the vector fields of continuous dynamical systems from numerical scalar time series, *Physical Review A* **43**, 5321 (1991).
- [12] G. Gouesbet and J. Maquet, Construction of phenomenological models from numerical scalar time series, *Physica D: Nonlinear Phenomena* **58**, 202 (1992).
- [13] G. Gouesbet, L. Le Sceller, C. Letellier, R. Brown, J. Buckler, and Z. Kollath, Reconstructing a dynamics from a scalar time series, *Annals of the New York Academy of Sciences* **808**, 25 (1997).
- [14] V. Petrov, J. Kurths, and N. Georgiev, Reconstructing differential equation from a time series, *International Journal of Bifurcation and Chaos* **13**, 3307 (2003).
- [15] N. Tsutsumi, K. Nakai, and Y. Saiki, Constructing differential equations using only a scalar time-series about continuous time chaotic dynamics, *Chaos: An Interdiscip. J. Nonlinear Sci.* **32**, 091101 (2022).
- [16] F. Christiansen, P. Cvitanovic, and V. Putkaradze, Spatiotemporal chaos in terms of unstable recurrent patterns, *Nonlinearity* **10**, 55 (1997).
- [17] M. C. Mackey and L. Glass, Oscillation and chaos in physiological control systems, *Science* **197**, 287 (1977).
- [18] M. Yamada and K. Ohkitani, Lyapunov spectrum of a chaotic model of three-dimensional turbulence, *Journal of the Physical Society of Japan* **56**, 4210 (1987).
- [19] A. Pikovsky, M. Rosenblum, and J. Kurths, Synchronization: a universal concept in nonlinear science (2002).
- [20] F. Takens, Dynamical systems and turbulence (1981).
- [21] T. Sauer, J. A. Yorke, and M. Casdagli, Embedology, *J. Stat. Phys.* **65**, 579 (1991).
- [22] D. Sweet, H. E. Nusse, and J. A. Yorke, Stagger-and-step method: Detecting and computing chaotic saddles in higher dimensions, *Phys. Rev. Lett.* **86**, 2261 (2001).
- [23] S. Kawano and S. Konishi, Nonlinear regression modeling via regularized gaussian basis function, *Bulletin of Informatics and Cybernetics* **39**, 83 (2007).
- [24] K. Ohkitani and M. Yamada, Temporal intermittency in the energy cascade process and local lyapunov analysis in fully-developed model turbulence, *Progress of theoretical physics* **81**, 329 (1989).
- [25] A. S. Pikovsky and P. Grassberger, Symmetry breaking of coupled chaotic attractors, *J. Phys. A:Math. Gen.* **24**, 4587 (1991).

Appendix A: Stagger-and-Step method using the delay-structures

Stagger-and-step method [22] is to create a “long trajectory” as the patch of segments of a short trajectory. The method is employed to create a long trajectory on a chaotic saddle by using the delay-structures (5). As seen in Fig. 7 a model trajectory created from the simple integration of the model by using the Runge-Kutta method approximates the actual one for times 400, whereas a trajectory created from the Stagger-and-Step method approximates the actual one for more than times 1000.

We describe the Stagger-and-Step method which we employ in Section IV. The basic steps of the Stagger-and-Step method [22] are as follows. See also Algorithm 1.

1. Calculate short numerical trajectories from nearby 100 initial conditions.
 - a Add noise to the current point with Algorithm 2.
 - b Calculate a numerical trajectory of length $T = 50$.
2. Choose the best trajectory among 100 trajectories. Trajectories are evaluated by the maximum delay absolute error:
$$E := \max_{t \leq 50 - \tau, i=1, \dots, D-1} |X_i(t) - X_{i+1}(t + \tau)|.$$
3. Keep the former half ([0,25]) of the best trajectory as an orbit segment.
4. Back to 1.

To reduce the number of trials in step 1, if the maximum delay absolute error E is less than a certain threshold $\Delta_{\text{threshold}}$ on step 1-b, we move on to step 2 even though the number of calculated numerical trajectories does not reach 100. Furthermore, before step 1 we calculate a numerical trajectory of length $T = 50$ without adding noises, and steps 1 and 2 are skipped if $E < \Delta_{\text{threshold}}$.

In our computations, we slightly modify Algorithm 1 to reduce computational costs. When the error becomes smaller with some noise, we search for a better noise by making additional noises around the original noise. Using this optimization, an appropriate noise can be gotten with lower computational costs and a long trajectory on a chaotic saddle can be made in a plausible time.

Algorithm 1 Refined Algorithm of Stagger-and-Step method

- 1: **for** $j = 0$ to 100 **do**
 - 2: **if** $j \geq 1$ **then**
 - 3: Add noise to the current point with Algorithm 2.
 - 4: **end if**
 - 5: Calculate a numerical trajectory $T = 50$.
 - 6: **if** $\max |X_i(t) - X_{i+1}(t + \tau)| < \Delta_{\text{threshold}}$ **then**
 - 7: Choose this trajectory as the best trajectory and go to 11.
 - 8: **end if**
 - 9: **end for**
 - 10: Choose the best trajectory among 101 trajectories concerning the maximum delay absolute error: $|X_i(t) - X_{i+1}(t + \tau)|$ ($i = 1, \dots, D - 1$).
 - 11: Keep the former half ([0,25]) of the best trajectory as an orbit segment.
 - 12: Back to 1.
-

Algorithm 2 Algorithm for noise making

- 1: Make a D -dimensional normally distributed vector \mathbf{v} .
 - 2: Make a scalar b which follows uniform distribution in $[-4, -1]$.
 - 3: **return** $10^b \frac{\mathbf{v}}{\|\mathbf{v}\|}$
-

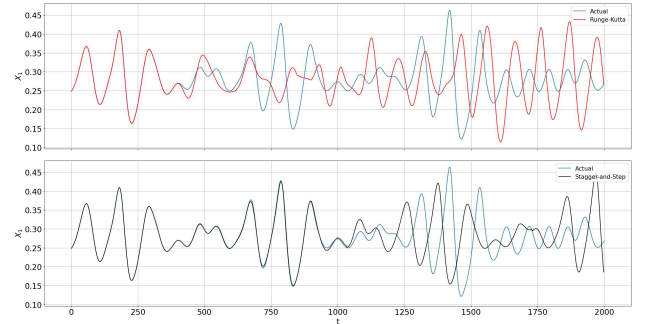


FIG. 7. Numerical trajectories of a data-driven model of the shell model dynamics computed from the simple calculation (upper panel) and the Stagger-and-Step method (lower panel). The blue line in each panel shows an actual trajectory. A trajectory generated using the Stagger-and-Step method is shown to approximate the actual trajectory more than times 1000, whereas a trajectory generated by simple integration of the model approximates the actual one for times 400. Note that a long trajectory created by the Stagger-and-Step method is actually a patch of short trajectories, but it seems “smooth”.

Appendix B: Relation between auto-correlation function and the choice of delay coordinate

We select the delay time τ by considering the decay of the auto-correlation function of a main variable. Figure 8 depicts auto-correlation functions of time s for the observable time series data of five examples. The adequate choice of τ should satisfy the correlation coefficient between $w(t)$ and $w(t - \tau)$ to be away from both 0 and 1. In fact, for each of the five successful examples, the correlation coefficient between $w(t)$ and $w(t - \tau)$ is KS:0.5012, MG:0.8011, SM:0.5357, CR: 0.9058, n-KS:0.4265.

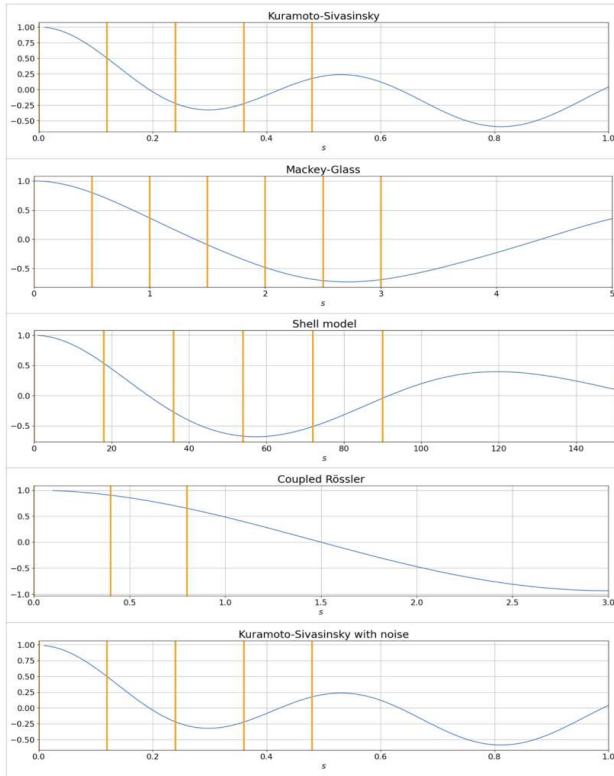


FIG. 8. **Auto-correlation function of a main variable.** The orange lines correspond to multiples of delay time τ used for the delay coordinates in Sections III and IV.

Appendix C: The estimation of time derivatives from a time series with noise

To estimate time derivatives from time series data, we employ the Taylor approximation. As mentioned in section II B, it is important to take a time step $l\Delta t$ larger when the observations include noise. Recall that $l\Delta t$ is a time step used to estimate time derivatives, where l is a positive integer and Δt is a time step of observed time series data.

In Fig. 9 we show the Taylor approximations at some points of the Kuramoto-Sivashinsky equation with noise. These approximations are used to estimate time derivatives. The estimates with a larger time step $l\Delta t$ for $l > 1$ tend to obtain better approximations under the existence of observation noise.

In Fig. 10 we depict the standard deviations of estimation errors in the time derivatives with respect to the value of l . The minimum standard deviations of the second-order and the sixth-order approximations are 0.866 and 0.833, respectively. We can robustly obtain a better estimation of time derivatives for a broader range of l when we apply the sixth-order approximation.

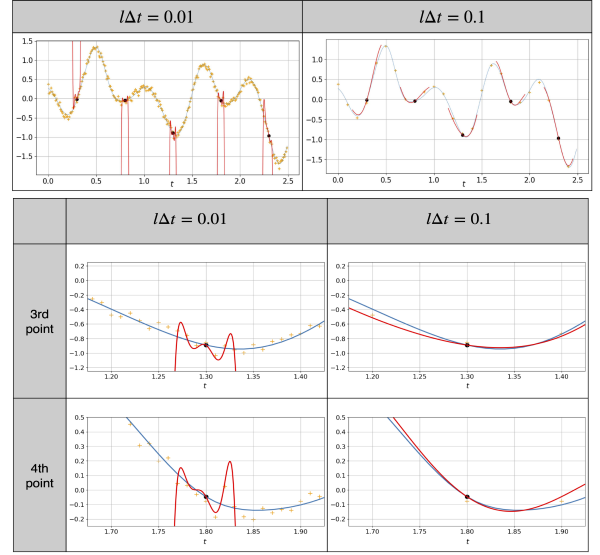


FIG. 9. **The sixth order Taylor approximation of a trajectory of the main variable (ω_1) at some sample points for the Kuramoto-Sivashinsky equation with noise (upper) and their enlarged pictures around two sample points (lower).** The blue line represents the time series of the Kuramoto-Sivashinsky equation and the orange points represent noised observable data. The red curve represents the Taylor approximation at each sample point (\bullet). The left panels employ observation points at every $l\Delta t = 0.01$ time step, whereas the right panels at every $l\Delta t = 0.1$ time step. For each of the two sample points in the lower panel, the estimation of the time derivative for the case of $l\Delta t = 0.1$ (right) is better than that of $l\Delta t = 0.01$ (left). In order to avoid the noise effect we need to choose a large value of l to estimate a time derivative at a sample point.

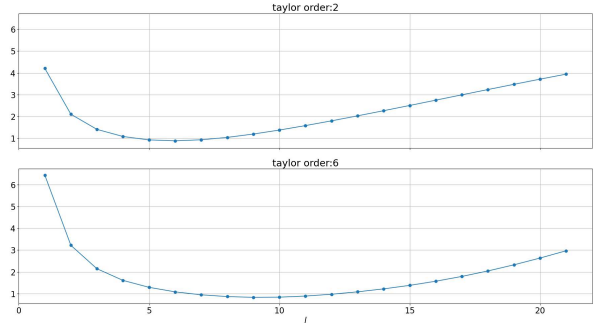


FIG. 10. **Standard deviations of the estimation errors in the time derivative with respect to l used to estimate time derivatives for the two cases using the second and the sixth order Taylor approximation.** The two panels show the standard deviations of the estimation error of the time derivative at 10^6 points on a trajectory. The upper panel employs the second-order Taylor approximation, and the minimum error value 0.866 is taken at $l = 6$. The lower panel employs the sixth order, the minimum error 0.833 is taken at $l = 9$. The standard deviation of error for the sixth-order Taylor approximation tends to take a low value for a broader range of l .

Appendix D: Short trajectories from several initial conditions

In Section IV, we show a single short trajectory for each case in Fig. 3. Here, we depict additional four short trajectories from randomly selected initial conditions for each of the data-driven models in Figures 11,12,13,14, and 15. These figures show that each model can predict short time trajectories appropriately independent of the initial conditions, which implies the validity of each model.

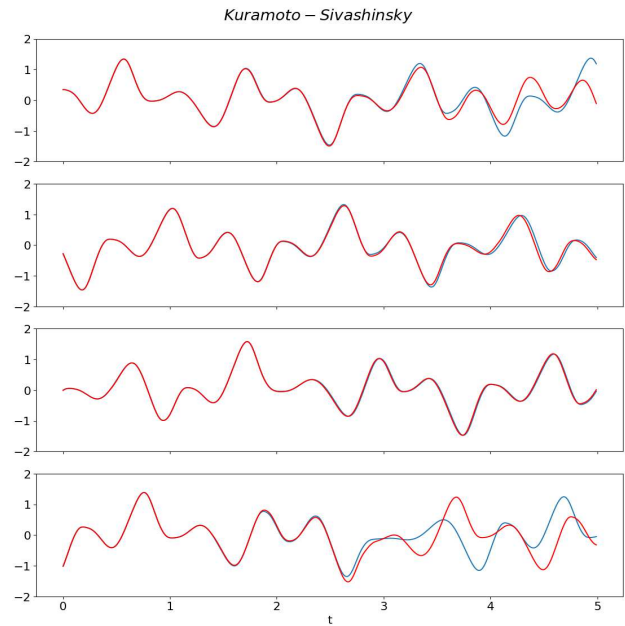


FIG. 11. Short time trajectories of X_1 of a data-driven model for Kuramoto-Sivashinsky equation. Blue and red indicate the cases for the actual and the model, respectively. Initial conditions are selected randomly from actual dynamics.

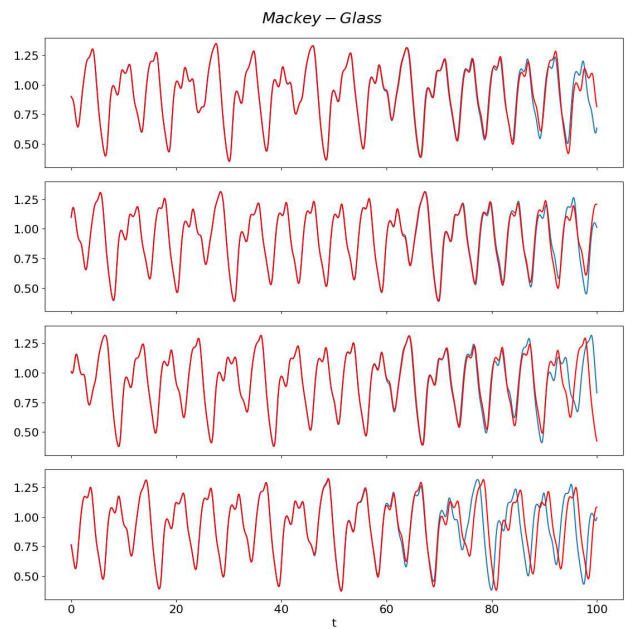


FIG. 12. Short time trajectories of X_1 of a data-driven model for Mackey-Glass equation. Blue and red indicate the cases for the actual and the model, respectively. Initial conditions are selected randomly from actual dynamics.

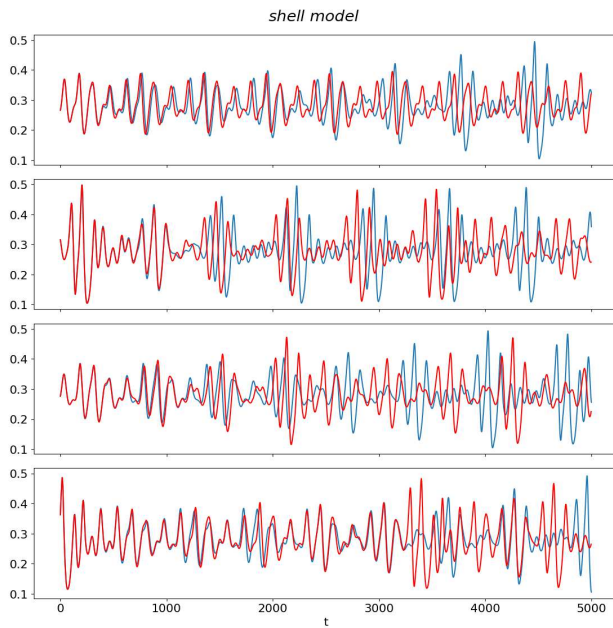


FIG. 13. Short time trajectories of X_1 of a data-driven model for shell model. Blue and red indicate the cases for the actual and the model, respectively. Initial conditions are selected randomly from actual dynamics.

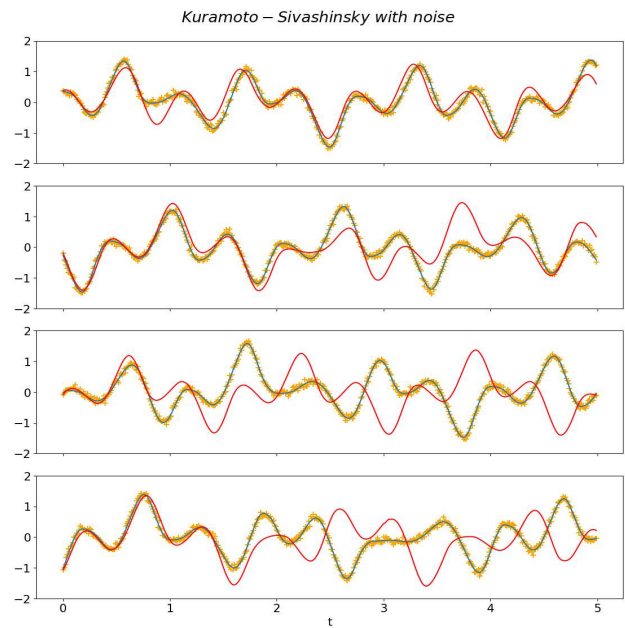


FIG. 15. Short time trajectories of X_1 of a data-driven model for Kuramoto-Sivashinsky equation with noise. Blue and red indicate the cases for the actual and the model, respectively and yellow points are observations with noise. Initial conditions are selected randomly from actual dynamics.

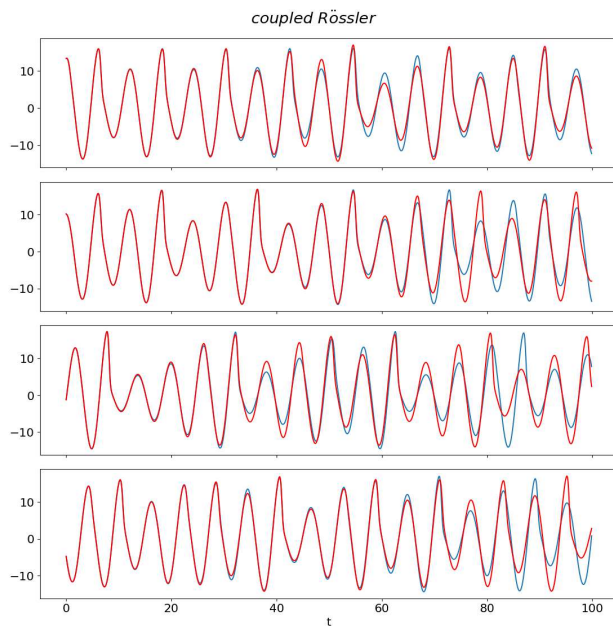


FIG. 14. Short time trajectories of X_1 of a data-driven model for coupled Rössler equation. Blue and red indicate the cases for the actual and the model, respectively. Initial conditions are selected randomly from actual dynamics.